NBI Suppression in Non-Linear UWB Channels using Second Order CPP-ANF

Farhana Begum, Manash Pratim Sarma
Kandarpa Kumar Sarma
Gauhati University
Department of Electronics and
Communication Engineering
Guwahati-781014, Assam, India
email-farhanajubi@gmail.com,manashpelsc@gmail.com
kandarpaks@gmail.com

Nikos Mastorakis
Technical University - Sofia
Sofia 1000, "Kl. Ohridski" 8, Bulgaria
mastor@tu-sofia.bg

Abstract: UWB systems are continuously affected by narrow band interference (NBI) emanating from traditional sources for which its mitigation continues to be a challenging issue. This is more so if the channels are considered to be non-linear which in reality is the actual scenario. NBI suppression is an essential element for achieving appropriate quality of service (QoS) and ensuring link reliability. Here, we report the design of a second-order adaptive notch filter (ANF) based scheme designed for suppression of single and multiple NBI in non-linear channel condition used by UWB systems. The proposed second order ANF uses a gradient descent adaptation in combined pipelined-parallelism (CPP) approach demonstrating reduced computational complexity and lower power requirement for an efficient hardware design. The CPP mode is ascertained after performing certain experiments using a number of digital filter design approaches like direct, cascade etc. Further, the system is also tested under IEEE 802.15.3a CM1, CM2, CM3, and CM4 channels.

Key–Words: UWB, NBI, ANF, CPP, non-linear, NARMA

1 Introduction

Ultra wideband (UWB), with extremely low power spectral density (PSD) of -41.25 dBm/MHz covering a large segment in the GHz spectrum, has been accepted to be a reliable option for high data rate wireless personal area networks (WPAN). The advantages of UWB like very high data-rate, low-cost and low-complexity transceiver design [1], [2] and its proliferation has resulted in the lunching of several modified versions. The impulse radio (IR) UWB together coined as IR-UWB is one such common version. Another variation considers the integration of time hopping into the IR-UWB systems. Pulse Position Modulation (PPM) is most commonly used for this purpose providing time hopping (TH). This results in TH-IR-UWB systems. Despite these variations and further improvement in the reception approaches of UWB system, there are several issues posing challenges. Among them, one arises from commonly occurring narrow band wireless sources which have much higher transmitted signal strength than the UWB systems. The narrow band interferences (NBI) produced by already existing narrow band (NB) systems always threaten to lower the quality of service (QoS) of UWB systems. Common NBI sources are Bluetooth, 3G/4G systems mobile radio system, digital audio broadcasting (DAB), IEEE 802.11, HyperLAN, etc. Enhancing QoS has been a continuous process as observed by works like [3]- [4]. The common approach to resolve such NBIs is to use fixed notch filters (NF) [5] with a zero gain at NBI frequency. But in cases where the NBI frequency is unknown [6], [7], or the channel behavior contains time-varying attributes, adaptive notch filter (ANF) based methods are required.

Another aspect observed in case of UWB systems is the fact that the channel is often assumed to be linear. In the true sense, it is highly non-linear. Therefore, most of the assumptions made while considering a highly non-linear system to be linear makes the system suffer from several shortcoming. UWB systems being a GHz range technology uses short-duration pulse for which timing and synchronization aspects require near distortion free mechanisms. Here, suppression of NBI becomes a critical aspect.

Although several ANF based schemes have been reported for estimation and recovery of TH-IR-UWB signals [8]-[11], none have been used for energy detection synchronization in non-coherent receiver designs. Further, none of the works have explored the

effectiveness of a second order ANF in combined pipelining parallelism (CPP) mode in mitigating NBI effects with detailed analysis of results obtained from certain known channel models and with stress on architectural dimensions with a view to ascertain the proper structure for practical implementation. Here, we propose a second-order ANFs for NBI mitigation for supporting distortion free synchronization in non-coherent energy detection receivers of TH-IR-UWB systems. The proposed second order ANF uses a gradient descent method in CPP approach with reduced computational complexity and requires lower power for an efficient hardware design. In terms of implementation, several schemes for realization like direct, cascade, lattice ladder, bi-quad, parallel and CPP are tested before finalizing the design. Further, the system is also tested under IEEE 802.15.3a CM1, CM2, CM3, and CM4 channels. The system performs single to multiple NBI cancelation with lower computational complexity and requires lower power for an efficient hardware design. Field grid programmable array (FPGA) based implementation of the system shows that the system is suitable for practical design. Some of the earlier works have been reported in [12]- [14].
The rest of the paper is organized as follows. In Section 2 the proposed approach of NBI suppression is discussed. It includes discussion on signal, channel, working of the system etc issues. Section 3 describes the implementation issues with stress on the process of selecting the CPP approach for its use in the present method. Results and related details are included in Section 4. The work is concluded in the Section 5.

2 Proposed NBI Suppression Method using CPP-ANF in Non-Linear Channels

The proposed work is described in the following subsections. It considers the signal and channel model and outlines the basic steps of the design.

2.1 Signal and Channel Models

The time hopping pulse position modulation (TH-PPM) modulation based UWB system in additive white Gaussian noise (AWGN) and IEEE 802.15.3a (wideband personal area networks standard) channel has a transmitted signal $S_{tr}(t)$ given as

$$S_{tr}(t) = \sum_{i} \sum_{n=0}^{N_c-1} \sqrt{E}_s g(t - nT_f - c_n^i T_c - \delta d_i - iN_s T_f) \quad (1)$$

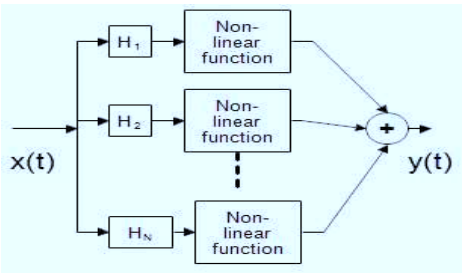

Figure 1: Schematic for applying non-linear channel effects in the trasmission

where $g(t)$ is the second order Gaussian derivative, E_s is the energy normalized transmitted UWB pulse in T_c is the chip duration, T_f is the frame duration, d_i is the i_{th} data bit, i is the bit index and N_s is the length of the TH-PPM in the repetitive coder.
With a system response of $y_i(t)$ to an input signal $x_i(t)$, a nonlinear channel generated as shown in Figure 1 is expressed as

$$H_{(p,q)} = \sum_{i=0}^{i=p} x(p) + \sum_{i=0}^{i=q} y(q) \quad (2)$$

where $x(p)$ are the zeros and $y(q)$ are zeros of a Non-Linear Auto-Regressive Moving Average (N-ARMA) process given as

$$y(t) = \prod_{i=1}^{i=N} H_{(p,q)}(t)x(t) \quad (3)$$

The non-linear channel attributes are modeled using NARMA considerations by feeding a common signal $x[n]$ to a system as shown in Figure 2. The blocks Ch_1 to Ch_N are path gains simulated using theoretical considerations. We have considered IEEE 802.15.3a CM1, CM2, CM3, and CM4 channels and Rayleigh fading as applicable to UWB channels. The blocks H_1 to H_N are infinite impulse response (IIR) filters combined with non-linear functions $(f(.)^2)$ configured to adaptively track the variations in the known channels Ch_1 to Ch_N. After the adaptation is complete, for each set of experiments such a channel block (among H_1 to H_N) is used to ascertain the performance of the system while executing NBI cancelation.

2.2 UWB Channels

The accurate design of channel model is a significant issue for certain UWB applications like WPAN communication system. Such a model creates the facility for calculation of large and small-scale statistics. Specifically, large-scale models are necessary for network planning and link budget design and small-scale

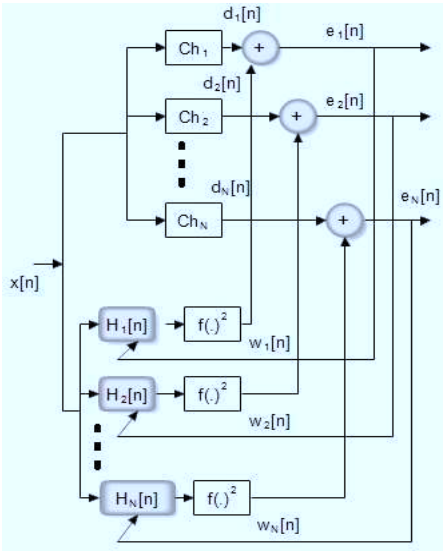

Figure 2: NARMA model of non-linear channel paths

models are necessary for efficient receiver design. The most famous multipath UWB indoor channel models are tapped-delay line Rayleigh fading model, Saleh and Valenzuela (SV) model and K model. The three most distinguishing features of such channels are [15]:

- The SV channel measurement shows that the multipath components are arriving in a cluster form. The different paths of such wide band signal can rise to several multipath components, all of which will be part of one cluster. The arrival of multipath components is modeled by using Poisson distribution with $\bigwedge$ (cluster arrival rate) and thus the inter arrival time between multipath components is based on exponential distribution. Further, the multipath arrival of UWB signals are grouped into two categories: cluster arrival and ray arrival within a cluster. This model requires several parameters to describe indoor channel environments. Ray arrival rate is the arrival rate of path within each cluster. The cluster arrival rate is always smaller than the ray arrival rate. The rays are also Poisson distributed with rate λ (ray arrival rate), and $\lambda >> \bigwedge$. The first ray is assumed to be arrived with no delay ($\tau_{0,l} = 0$).

- The amplitude statistics in SV model are based on log-normal distribution, the power of which is controlled by the cluster and ray decay factor. The total multipath energy is captured by the term x_i, the total energy contained in the multipath gain coefficients $\alpha_{k,l}$ may be normalized. The shadowing term is characterized by

$$20log(X_i) \infty (0, \sigma^2)$$

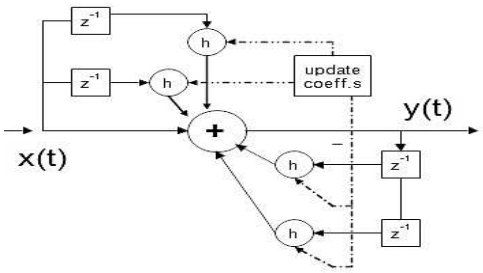

Figure 3: Proposed second order ANF

Indoor channel environments are classified as CM1, CM2, CM3, and CM4 following IEEE 802.15.3a standard based on propagation conditions as follows. To study the delay characteristics of the modified S-V channel under UWB, the impulse response of the channels are studied. Certain characteristics of the channels are as below:

- CM1 describes a line-of sight (LOS) scenario with a maximum distance between transmitter and receiver of less than 4 m.

- CM2 describes the same range as of CM1, but for a non-line-of sight (NLOS) situation.

- CM3 describes a NLOS medium for separation between transmitter and receiver of range 4-10 m.

- CM4 describes an environment of more than 10 m with strong delay dispersion, resulting in a delay spread of 25 ns with NLOS medium.

The characteristics of these channels are summarized in Table 1.

2.3 Second order ANF

The most critical section of the proposed NBI cancelation is the design of the second order ANF. The primary feature of the proposed design are its ability to adaptively track the signal, high speed processing and low power requirements. The proposed design is based on a second order ANF which has an adaptive update algorithm necessary for tracking the signal. The second order structure provides better contextual processing than a first order form thereby accelerates the learning. A second order IIR ANF as shown in Figure 3 is used as the primary element to cancel the NBI. Each notch filter has two pairs of pole-zeros. The transfer function of second order ANF is expressed as

$$H(z) = \frac{A(z)}{B(z)} = \frac{1 - \alpha z^{-1} - \alpha z^{-2}}{1 - \beta z^{-1} - \beta z^{-2}} \qquad (4)$$

Table 1: Comparison parameters of UWB Channels

Channel Characteristics	$CM1$	$CM2$	$CM3$	$CM4$
Cluster arrival rate $\frac{1}{\Lambda}$ ($\frac{1}{nsec}$)	0.0233	0.4	0.0667	0.0667
Ray arrival rate ($\frac{1}{\Lambda}$) ($\frac{1}{nsec}$)	2.5	0.5	2.1	2.1
Cluster decay factor ($\frac{1}{\Gamma}$) ($\frac{1}{nsec}$)	7.1	5.5	14.00	24.00
Ray decay factor $\frac{1}{\gamma}$ ($\frac{1}{nsec}$)	4.3	6.7	7.9	12
Standard deviation of cluster lognormal fading term (dB)($\frac{1}{\sigma_1}$)	3.3941	3.3941	3.3941	3.3941
Standard deviation of ray lognormal fading term (dB) ($\frac{1}{\sigma_2}$)	3.3941	3.3941	3.3941	3.3941
Standard deviation of lognormal shadowing term (dB) ($\frac{1}{\sigma_x}$)	3	3	3	3

where α denotes complex value zero, β denotes complex value poles. The pole is located as close to the unit circle. The complex valued pole is represented by the expressions $\alpha = e^{j\Omega}$ and $\beta = re^{j\Omega}$ where r denotes the pole radius of the filter and Ω is the notch angular frequency.

$$H(z) = \frac{A(z)}{B(z)} = \frac{1 - e^{j\Omega}z^{-1} - e^{j\Omega}z^{-2}}{1 - re^{j\Omega}z^{-1} - re^{j\Omega}z^{-2}} \quad (5)$$

There is a deep notch at $\Omega = \Omega o$. It is supposed that the notch filter is shifted to an arbitrary position using frequency prediction and mapping. This work aims at designing a notch filter for suppression of NBI. The designed filter should place the notch at the detected NBI frequency. Thus, the transfer function at $e^{j\Omega_o}$ is expressed as

$$H(e^{j\Omega_o}) = \frac{1 - e^{j(\Omega-\Omega_o)} - e^{j(\Omega-\Omega_o)^2}}{1 - re^{j(\Omega-\Omega_o)} - re^{j(\Omega-\Omega_o)^2}} \quad (6)$$

The value of r is closely taken as one, the response of the transfer function is invariable with unit gain. $|H(e^{j\omega_o})|_{\Omega=\Omega_o \approx 0}$. So, the response of the filter is invariable with a unit gain except at $\Omega \sim \Omega_o$ with a deep notch. This design implies that the desired filter has a notch at the detected NBI frequency and is capable of removing the NBI component leaving other components unchanged. Here, r controls 3 dB bandwidth which is crucial for canceling the NBI. The difference expression between the output $y(k)$ and input notch filter $x(k)$ is

$$y(k) = x(k) - e^{jw(k)}x(k-1) - a1 - a2 \quad (7)$$

where $a1 = re^{jw(k)}y(k-1)$, $a2 = re^{jw(k)}y(k-2)$, $x(k)$ $(k = 1, 2\ldots)$ is a complex valued sequence including the UWB waveform, NBIs and white noise. The input samples are given as

$$x(k) = x_i(k) + x_q(k) \quad (8)$$

where $x_i(k)$ and $x_q(k)$ are the in-phase and quadrature sampling series respectively. Further, $y(k)$ is the complex valued output of the notch filter and $w(k)$ is the k^{th} angular frequency. The output of $A(z)$ is an error signal and is given as

$$e_w(k) = x(k) - e^{jw(k)}x(k-1) - e^{jw(k)}x(k-2) \quad (9)$$

The cost function using mean square error (MSE) becomes

$$J(w) = E[e_w(k)e_w^*(k)] \quad (10)$$

The variable coefficient is updated to minimize the cost function. The weight iteration $J(w)$ is updated with respect to w. It is given as

$$\begin{aligned}
&\delta J(w)/\delta(w) \quad (11)\\
&= E[-je^{jw(k)}x^*(k-1)x(k) + je^{jw(k)}\\
&x^*(k-1)x(k) + je^{jw(k)}x^*(k-2)x(k)]\\
&= E[-je^{jw(k)}x^*(k-1)x(k)]^*\\
&+ [-je^{jw(k)}x^*(k-1)x(k)]\\
&+[-je^{jw(k)}x^*(k-1)x(k)]\\
&= -2ImE[je^{jw(k)}x^*(k-1)x(k)\\
&+ je^{jw(k)}x^*(k-2)x(k)]
\end{aligned}$$

The adaptive weight coefficient update process is expressed as

$$w(k+1) = w(k) + \mu Im[a3 + a4] \quad (12)$$

where $a3 = e^{jw(k)}x^*(k-1)x(k)$, $a4 = e^{jw(k)}x^*(k-2)x(k)$ and μ is the step size controlling the convergence rate which facilitates the frequency tracking in linear and non-linear channels. The functioning of the entire system is summarized in Figure 4. The working of the receiver is linked to several stages. First, frame synchronization happens. Several parallel buffers in an array ensures frame synchronization. The buffers store signal samples at different clock cycles within the given timing window. Out of these samples, the maximum energy signal is selected. It

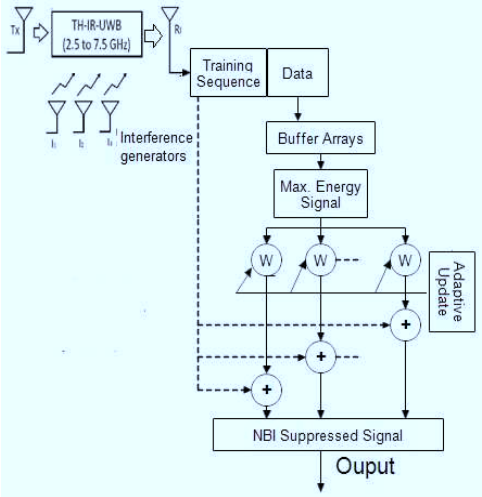

Figure 4: Receiver structure

is passed through a block of CPP ANFs designed to work together with energy detection based synchronization. Next, symbol synchronization is performed which is essential for recovery of the data bits. It ensures NBI is suppressed and synchronization is effectively done. A pipelining process is applied. Pipelined processing reduces power consumption by distributing the supply voltage along different clock cycles. Further, the parallel processing speeds up the execution process which is essential for a extremely narrow timing cycle based system like UWB. In the next section, we describe the process of NBI cancelation executed in CPP mode and the related details.

3 Implementation of NBI Cancelation in CPP Mode

The CPP mode provides certain advantages which shall be obvious from the discussion below and the experiential results described in the subsequent sections. We perform a series of experiments and explore several traditional digital filter design approaches before finalizing the design for the implementation of second order ANF. Here, we describe the implementation of direct, cascade, lattice ladder, bi-quad, parallel and CPP approaches before fixing the design.

3.1 Direct form Realization

The representation for direct form realization is given as:

$$y[n] = \sum_{k=0}^{k=N} b[k]x[n-k] - \sum_{k=1}^{k=N} a[k]y[n-k] \quad (13)$$

This form of realization is very convenient for software implementation. However, it suffers from some disadvantages like sensitivity to accuracy of realized coefficients as it is affected by the largest finite word-length effect as well as and the greatest complexity due to implementation which needs most resources. In terms of hardware implementation, the area required for direct form is found to be exponentially increasing as data rate increases.

3.2 Cascade form Realization

By expressing the numerator and the denominator polynomials of the transfer function as a product of polynomials of lower degree, a digital filter can be realized as a cascade of low-order filter sections. The representation for cascade form realization is given as:

$$H(z) = \frac{P(z)}{D(z)} \quad (14)$$

where $P(z) = P_1(z).P_2(z).P_3(z)$ and $Q(z) = Q_1(z)Q_2(z)Q_3(z)$ Usually, the polynomials are factored into a product of first order and second order polynomials. The fabrication area required for to implement a cascade realization is more. Further, the number of processors required is more. This poses a major problem in hardware implementation necessitating a large amount of power dissipation.

3.3 Lattice Ladder form

Lattice ladder form is obtained by changing the inputs and outputs. Along with the signal flows, the signs of signals are also changed. This is also a recursive structure which can implement a IIR structure. The addition of finite number of zeroes results in a ladder form. The representation for lattice ladder form realization is given as

$$H(z) = \frac{\gamma_N(0) + \gamma_N(1)z^{-1} + \gamma_N(2)z^{-2} + \ldots}{1 + \alpha_N(1)z^{-1} + \alpha_N(2)z^{-2} + \ldots} \quad (15)$$

This form of realization is used for software implementation. However, this form of realization necessitates a much larger area for hardware implementation.

3.4 Bi-Quad Realization

High order ANF filters are highly sensitive to quantization of their coefficients and is thereby unstable. The problem is however less with first and second order filters. Therefore, higher order filters are typically implemented as serially-cascaded bi-quad sections. The two poles of the bi-quad filter must be inside the unit circle for it to be stable. This is true for

all filters. All poles must be inside the unit circle for the filter to be stable. The equation for second order ANF bi-quad section is represented as

$$d(n) = x(n) - a_1 d(n-1) - a_2 d(n-2) \quad (16)$$

$$y(n) = b_0 d(n) - b_1 d(n-1) - b_2 d(n-2) \quad (17)$$

where a_1 and a_2 are filter co-efficients and b_0 and b_1 and b_2 are pole coefficients respectively and d_n is an intermediate function. Analyzing the above expressions ((16) and (17)), it is noticed that the bi-quad implementation only requires four additions and five multiplications, which is accommodated on any modern micro-controller/ DSP. Also, implementing the direct form realization into two steps in the above significantly reduces the filters sensitivity to quantization error.

3.5 Parallel Realization

Parallel processing can reduce the power consumption of system by allowing the supply voltage to be reduced. In an L-parallel system, the charging capacitance does not usually change while the total capacitance is increases by L times. In order to maintain the same sample rate, the clock period of the L-parallel filter must be increased to LT_{seq}, where T_{seq} is the propagation delay of the sequential circuit. This means that C_{charge} is charged in time LT_{seq} rather than in time T_{seq}. In other words, there is more time to charge the same capacitance. This means that the supply voltage can be reduced to βV_o. The propagation delay can be used to compute the supply voltage of the L parallel system. The propagation delay of the original system is given by

$$T_{seq} = \frac{C_{charge} V_o}{k(V_o - V_t^2)} \quad (18)$$

while the propagation delay of the L parallel system is given by

$$LT_{seq} = \frac{C_{charge} V_o \beta}{k(\beta V_o - V_t^2)} \quad (19)$$

From the above equations ((18) and (19)), the following quadratic equation can be obtained to compute β, where $L(\beta V_o - V_t)^2 = \beta(V_o - V_t)^2$. Once β is computed, the power consumption of the L parallel system can be calculated as

$$P_{par} = LC_{charge}(\beta V_o)^2 \frac{f}{L} \quad (20)$$

$$= \beta^2 C_{charge} V_o^2 f \quad (21)$$

$$= \beta^2 P_{seq} \quad (22)$$

where P_{seq} is power consumption of the sequential system. Therefore, as in the pipelined system, the power consumption of the L parallel system has been reduced by a factor of β^2 as compared to the original system.

3.6 Combined Pipelining and Parallel

The propagation delay of T_{pd} of CMOS circuits is associated with charging and discharging of various gate and stray capacitances in the critical path [**?**]. For a CMOS circuits, the propagation delay is written as $T_{pd} = \frac{C_{charge} V_o}{k(V_o - V_t^2)}$, where C_{charge} denotes the capacitance to be charged/ discharged in a single clock cycle i.e the capacitance along the critical paths, V_o is the supply voltage and V_t is the threshold voltage. Parameter k is a function of technology, μ, w/l and c_{ox}. The power consumption can be estimated using the equation $P = C_{total} V_o^2 f$ where C_{total} denotes the total capacitances, V_o is the supply voltage and f is the clock frequency of the circuit.

3.6.1 Pipelined Approach

The power consumption is given

$$P_{seq} = C_{total} V_o^2 f \quad (23)$$

represent the power consumption in original filter. The value of $f = 1/T_{seq}$, where T_{seq} is the clock period of the original sequential filter. If an M-level pipelined system is considered, the critical path is reduced to $1\frac{1}{M}$ of its original length and the capacitance to be charged/discharged in a single clock cycle is reduced to C_{charge}/M. The total capacitance does not change. If the same clock speed is maintained i.e the clock frequency f is maintained, only a fraction of the original capacitance is C_{charge}/M is being charged discharged at the same amount of time that was previously needed to charge/discharge the capacitance C_{charge}. This implies then that the supply voltage can be reduced to β V_o where β is a positive constant less than 1 thereby the power consumption of the pipelined filter will be $P_{pip} = C_{total}\beta^2 V_o^2 f = \beta^2 P_{seq}$. Therefore, the power consumption has been reduced by a factor of $\beta^2 P_{seq}$ compared to the original system. The power consumption reduction factor β can be determined by examining the relationship between the propagation delay of the original filter and pipelined filter. The propagation delay of the original filter is given by:

$$T_{seq} = \frac{C_{charge} V_o}{k(V_o - V_t^2)} \quad (24)$$

The propagation delay of the pipelined filter is given by

$$T_{pip} = \frac{C_{charge} V_o \beta}{k(V_o - V_t^2)} \tag{25}$$

It is noteworthy that the clock frequency is set equal to the propagation delay T_{pd} in a circuit. Since the same clock speed is maintained for both filters the below the following quadratic equation can be used to solve β.

$$M(\beta V_o - V_t)_2 = \beta(V_o - Vt)^2 \tag{26}$$

3.6.2 Parallel Processing for Low Power

Parallel processing can reduce the power consumption of system by allowing the supply voltage to be reduced. In an L-parallel system, the charging capacitance does not usually change while the total capacitance is increases by L times. In order to maintain the same sample rate, the clock period of the L-parallel filter must be increased to LT_{seq}, where T_{seq} is the propagation delay of the sequential circuit. This means that C_{charge} is charged in time LT_{seq} rather than in time T_{seq}. In other words, there is more time to charge the same capacitance. This means that the supply voltage can be reduced to βV_o. The propagation delay can be used to compute the supply voltage of the L parallel system. The propagation delay of the original system is given by

$$T_{seq} = \frac{C_{charge} V_o}{k(V_o - V_t^2)} \tag{27}$$

while the propagation delay of the L parallel system is given by

$$LT_{seq} = \frac{C_{charge} V_o \beta}{k(\beta V_o - V_t^2)} \tag{28}$$

From the above equations ((27) and (28)), the following quadratic equation can be obtained to compute β, where $L(\beta V_o - V_t)^2 = \beta(V_o - V_t)^2$. Once β is computed, the power consumption of the L parallel system can be calculated as

$$P_{par} = LC_{charge}(\beta V_o)^2 \frac{f}{L} \tag{29}$$

$$= \beta^2 C_{charge} V_o^2 f \tag{30}$$

$$= \beta^2 P_{seq} \tag{31}$$

where P_{seq} is power consumption of the sequential system. Therefore, as in the pipelined system, the power consumption of the L parallel system has been reduced by a factor of β^2 as compared to the original system.

3.6.3 Combined Parallel and Pipelined

The techniques of pipelining and parallelism can be combined for lower power consumption. The principles remain the same i.e pipelining reduces the capacitances to be charged/ discharged in 1 clock period and parallel processing increases the clock period for charging/ discharging the original capacitance. The propagation delay of the parallel-pipelined filter as

$$)LT_{pd} = \frac{\frac{C_{charge}}{M} \beta V_o}{k(\beta V_o - V_t^2)^2)} \tag{32}$$

Using the equation ((32)) the following equation is obtained

$$ML(\beta V_o - V_t)^2 = \beta(V_o - Vt)^2 \tag{33}$$

It should be noted that the supply voltage cannot be lowered indefinitely even by applying more levels of pipelining and parallelism. There is a lower bound on the supply voltage that is dictated by the process parameters and noise margins.

4 Experimental Results, Discussion and Performance Comparison

Signals are transmitted in TH-IR-UWB form in a frequency range 2.5 GHz to 7.5 GHz corrupted by NBI sources like WLAN (5.2 GHz and 5.8 GHz) and RFID 6.8 Ghz. At the receiver, frame synchronization is performed initially using energy detection based receivers. The next step is NBI mitigation technique where ANF blocks are arranged in CPP mode of processing. Thereafter, symbol synchronization is performed followed by demodulation or data recovery using energy detection receivers. By varying the pole-radius r between 0 and 1, different responses of ANF are obtained which is necessary to determine the notch frequency of a case where signal details are unknown. The closer r is to unity, the wider will be the ANF response. Also, a smaller distortion will be obtained. So, r is called the distortion parameter which controls the 3 dB notch bandwidth.

Figure 5 shows the plot of least mean square error (LMSE) versus iteration with different step sizes of 0.09 and 0.009. The varying step-sizes illustrates the basic-trade-offs between rate of convergence and stability. The smaller step sizes increases the accuracy but make the process computationally intensive. Also there is a chance of over training. A proper choice of the step size depends upon the experimental conditions and is fixed using trial and error approach. The second order ANF structure ensures faster learning

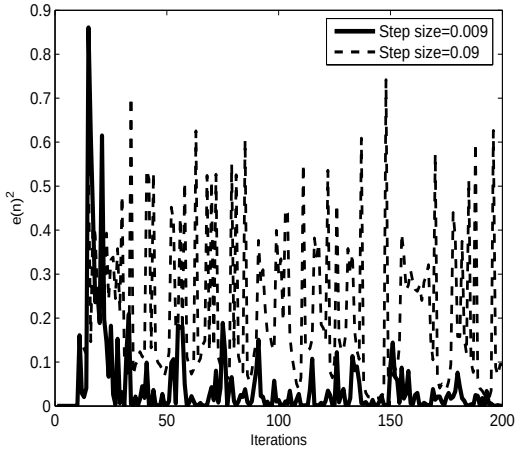

Figure 5: Step Size: $\mu = 0.09$ and $\mu = 0.009$

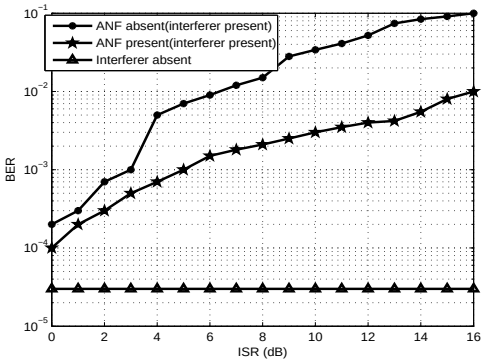

Figure 6: BER versus interference characteristics

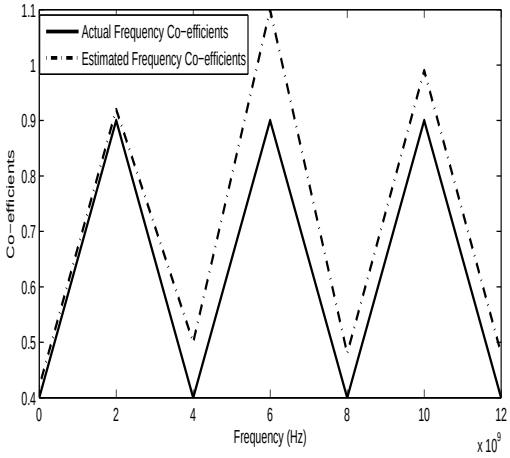

Figure 7: Comparison of estimated filter coefficients and actual coefficients

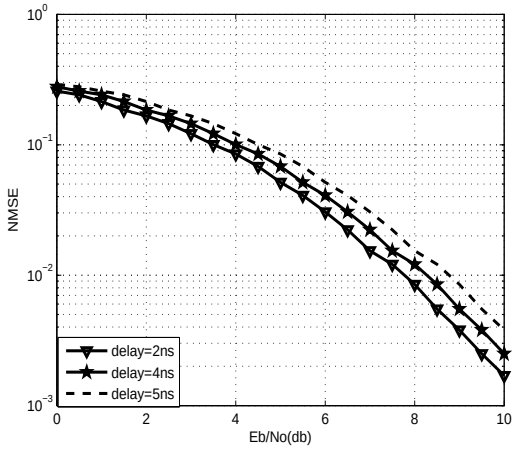

Figure 8: BER response of the curves with different timing delays

compared to a first order form due to higher cancelation of common moded terms. The multiple delayed feeds ensures that the most relevant portion of the data is circulated compared to a first order form. A comparison of this scheme is made in the presence of a CM1 channel in an interfering environment in terms of bit error rate (BER) against Interference to Signal ratio (ISR) is shown in Figure 6. The ANF used in conjunction with energy detection helps in improving the performance of the system by eliminating the strong NBI interference. This establishes the importance of ANF in suppressing NBI.

Figure 7 shows the plot of estimated filter-coefficients and actual coefficients. Figure 8 shows the synchronization system performance with timing jitters in terms of BER. Increasing the delay degrades the performance of the system. Thus, after a detailed analysis we find that the proposed CPP-ANF for TH-IR-UWB system shows better BER performance with lower computational complexity, higher stability, superior resilience against interference in stochastic non-linear channels with one to multi-order NBI sources and lower power requirement as verified using FPGA platforms. Table 2 gives an overall picture of filters used for multiple NBI suppression in terms of computational complexity and its associated parameters. The design in CPP mode has the least amount of computational complexity and lowest power requirement.

Fig. 9 gives the impulse responses of the IEEE 802. 15.3 channels. Figs. 10, 11, 12 and 13 represents interference suppression in a CM1, CM2, CM3 and CM4 channels respectively in an interference intercepted environment which is here considered due to the presence of three interference which are Zigbee (3.5 Ghz), WLAN (5.25 and 5.75 GHz) and RFID (6.8 Ghz). Clearly, the proposed system is able to deal with all the identified channel types and mitigates multiple NBI sources. Further, with lower computational complexity and lesser power requirements, it is a suitable

Table 2: Comparison parameters

Forms	Computational complexity	Power (mW)
$Direct$	12 multipliers, 4 adders	1.8
$Cascade$	9 multipliers, 3 adders	0.829
$ContinuedFraction$	6 multipliers, 6 adders	0.679
$Ladder$	3 multipliers, 2 adders	0.407
$Parallel$	3 multipliers, 2 adders	0.407
CPP	3 multipliers, 2 adders	0.407

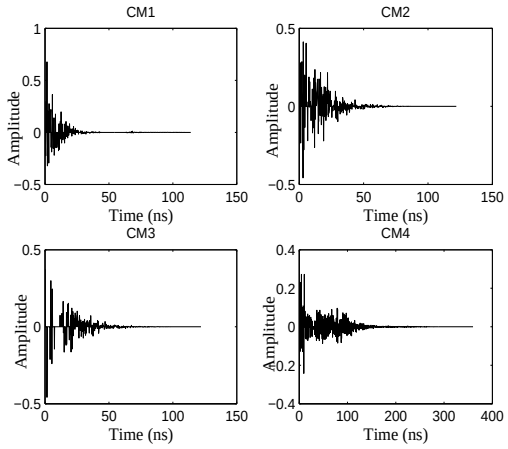

Figure 9: Impulse response of Channels

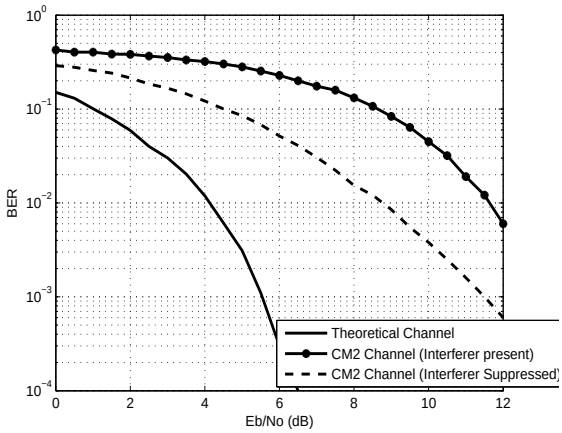

Figure 11: Interference Suppression in CM2 Channel

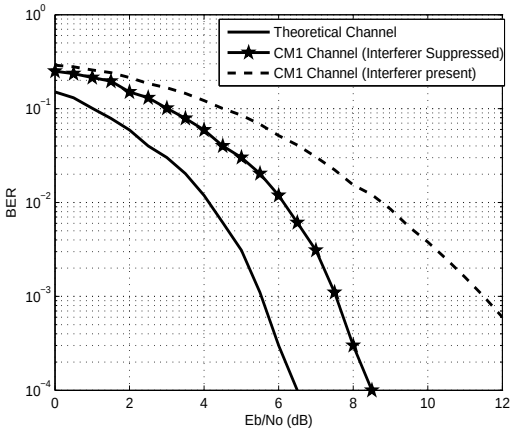

Figure 10: Interference Suppression in CM1 Channel

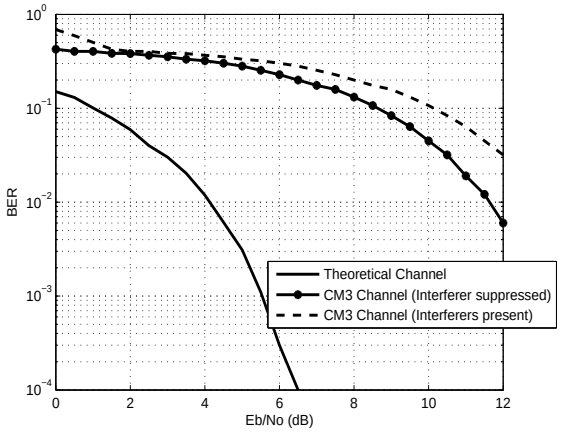

Figure 12: Interference Suppression in CM3 Channel

option for design of high data rate adaptive UWB receivers.

5 Conclusion

Here, we have reported the design of an ANF used for NBI mitigation in non-linear channels in case of signals transmitted using TH-IR-UWB system. The ANF is designed in the CPP mode for which it generates higher computational speed and lower power requirement. The ANF tracks the signals using a gradient descent algorithm which cancels out single and multiple NBIs. The power requirements have been verified using FPGA based implementation. Experimental results show that the system is suitable for practical applications with higher computational speed and lower power attributes.

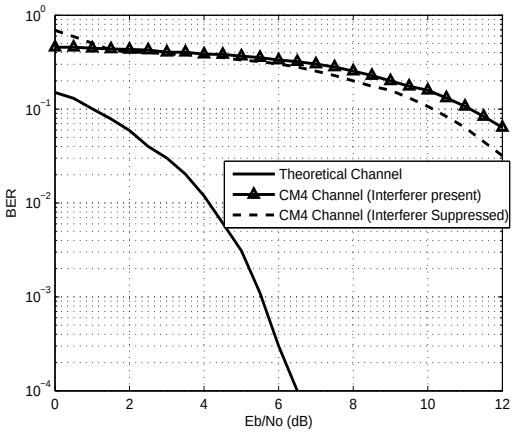

Figure 13: Interference Suppression in CM4 Channel

Acknowledgment

The authors acknowledge the support of Ministry of Communication and Information Technology, Govt. of India for facilitating the work.

References:

[1] J. Balakrishnan, A. Batra, and A. Dabak, "A multi-band OFDM system for UWB communication", in Proceedings of *IEEE Conference on Ultra Wideband System Technology*, Reston, Va, USA, pp. 354-358, November, 2003.

[2] L. Yang and G. B. Giannakis, "Ultra-wideband commu-nications, "An idea whose time has come", *IEEE Signal Processing Magazine*, vol. 21, no. 6, pp. 26-54, November, 2004.

[3] R. Bose, "On the performance of Turbo Codes over UWB channels at low SNR", *WSEAS Transactions on Communications*, vol. 2, no. 3, pp. 314-322, July, 2003.

[4] C. T. Manimegalai and R. Kumar, "Performance of LDPC- Coded APSK-Modulation for Wireless USB", *WSEAS Transactions on Communications*, vol. 12, no. 12, pp. 661-669, December, 2013.

[5] X.Lua, J-G-Mak, K.S Yeo and E-P Liu, "Compact ultra-wideband(UWB) bandpass filter with ultra-narrow dual and quad-notched banks", in *IEEE Transactions on Microwave Theory technology*, vol. 59, no. 6, pp. 1509-1519, June 2011.

[6] R. Ghatak, P. Sarkar, R.Mishra and D.Poddar, " A compact UWB bandpass filter with embedded SIR as notch structure", *IEEE Microwave Wireless Communication Letters*, vol. 21, no. 5, pp. 261-263, May 2011.

[7] W. Yu, Y. Shim and M.Rais-Zadeh, "Miniaturized UWB filters with tunable notch filters using a silicon-based integrated passive technology," in *IEEE Transactions on Microwave Theory Journal*, vol. 60, no. 3, pp. 518-527, March 2012.

[8] H. Xiong, W. Zhang, Z. Duo, B. He and D. Yuan, "Front-End Narrowband Interference Mitigation for DS-UWB Receiver", in *IEEE Transactions on Wirelesss Communications*, vol. 12, no. 13, September 2013.

[9] C. Jun Won and C. Nam, " Suppression of narrow band interference in DS spread spectrum using adaptive IIR notch filter," *IEEE Journal on Signal Processing*, vol. 54, no. 8, pp. 2003-2013, December 2002.

[10] M. Niewdwicky, " Tracking Analysis of a generalised Adaptive Notch Filter," *IEEE Journal on Signal Processing*, vol. 54, no. 1, pp. 304-314, January 2006.

[11] A. Regalia, "A Complex Adaptive Notch Filter," in *IEEE Signal Processing Letters*, vol. 17, no. 11, pp. 937-938, November 2010.

[12] F. Begum, M. P. Sarma and K. K. Sarma, "Preamble aided Energy Detection based Synchronization in Non-Coherent UWB Receivers", in Proceedings of *IEEE International Conference on Signal Processing and Integrated Networks* , Noida, India, February 2014.

[13] F. Begum, M. P. Sarma, K. K. Sarma and N. Mastorakis, "NBI Suppression in UWB System in Stochastic Non-Linear Channels", in Proceedings of 2^{nd} I*nternational Conference on Wireless and Mobile Communication Systems (WMCS14)*, Lisbon, Portugal, October 30 - November 1, 2014.

[14] F. Begum, M. P. Sarma, K. K. Sarma and N. Mastorakis, "Interference Suppression using CPP Adaptive Notch Filters for UWB Synchronization in Stochastic Non-Linear Channels", in Proceedings of *IEEE Symposium Series on Computational Intelligence (SSCI 2014)*, Orlando, Florida, USA, December, 2014.

[15] A. F. Molish, "Ultra-wideband Propagation Channel Theory, Measurement and Modeling", IEEE Transactions on Vehicular Technology, vol. 54, no. 5, pp. 1528-1545, 2005.